Ocean acidification over the next three centuries using a simple global climate carbon-cycle model: projections and sensitivities.

C. A. Hartin*, B. Bond-Lamberty, P. Patel and Anupriya Mundra

Pacific Northwest National Laboratory, Joint Global Change Research Institute at the University of Maryland-College Park, 5825 University Research Court #3500, College Park, MD 20740, USA

*Corresponding author: Corinne.hartin@pnnl.gov

ABSTRACT

Continued oceanic uptake of anthropogenic CO_2 is projected to significantly alter the chemistry of the upper oceans over the next three centuries, with potentially serious consequences for marine ecosystems. Relatively few models have the capability to make projections of ocean acidification, limiting our ability to assess the impacts and probabilities of ocean changes. In this study we examine the ability of Hector v1.1, a reduced-form global model, to project changes in the upper ocean carbonate system over the next three centuries, and quantify the model's sensitivity to parametric inputs. Hector is run under prescribed emission pathways from the Representative Concentration Pathways (RCPs), and compared to both observations and a suite of Coupled Model Intercomparison (CMIP5) model outputs. Current observations confirm that ocean acidification is already taking place, and CMIP5 models project significant changes occurring to 2300. Hector is consistent with the observational record within both the high (>55°) and low latitude oceans (<55°). The model projects low latitude surface ocean pH to decrease from preindustrial levels of 8.17 to 7.77 in 2100, and to 7.50 in 2300; aragonite saturations decrease from 4.1 units to 2.2 in 2100 and 1.4 in 2300 under RCP 8.5. These

magnitudes and trends of ocean acidification within Hector are largely consistent with the CMIP5 model outputs, although we identify small biases within Hector's carbonate system. Modeled changes in pH are sensitive to those parameters that directly affect atmospheric CO_2 concentrations (beta and Q_{10}), while changes in Ω_{Ar} saturation levels are sensitive to changes in ocean salinity and Q_{10}. We conclude that Hector is a robust tool well-suited for rapid ocean acidification projections, sensitivity analyses, and is capable of emulating both current observations and large scale climate models under multiple emission pathways.

1. INTRODUCTION

Human activities have led to increasing anthropogenic emissions of greenhouse gases to the atmosphere. In the first decade of the 21st century CO_2 emissions from anthropogenic sources and land use changes accounted for ~9 Pg C yr^{-1}, with future emission projections of up to 28 Pg C yr^{-1} by 2100 under Representative Concentration Pathway 8.5 (RCP 8.5) (Riahi et al., 2011). The world's oceans have played a critical role in lessening the effects of climate change by absorbing 25-30% of the total anthropogenic carbon emissions since 1750 (Le Quéré et al., 2013; Sabine et al., 2011).

In response to this increasing atmospheric burden of CO_2 and increasing oceanic uptake, the oceans are experiencing both physical and biogeochemical changes: surface and deep water warming, reduced subsurface oxygen, and a reduction in calcium carbonate saturation levels and pH (Doney, 2010). Mean surface ocean pH has decreased by 0.1 units relative to preindustrial times (Caldeira et al., 2003). If current emission trends continue, ocean acidification will occur at rates and extents not observed over the last few million years (Feely et al., 2004; Feely et al., 2009; Kump et al., 2009; Caldeira et al., 2003). Ocean acidification occurs when atmospheric CO_2 dissolves in seawater ($CO_2(aq)$), forming carbonic acid (H_2CO_3), dissociating into carbonate (CO_3^{2-}) and bicarbonate (HCO_3^-), and releasing protons (H+). The net effect of adding CO_2 to the system increases the concentrations of [H_2CO_3], [HCO_3^-], and [H^+], while decreasing [CO_3^{2-}] concentrations and lowering the pH. The sum of [HCO_3^-], [CO_3^{2-}] and [CO_2^*], where [CO_2^*] = [$CO_2(aq)$] + [H_2CO_3] represents the total inorganic carbon or dissolved inorganic (DIC) of the system. As $CO_2(aq)$ continues to increase in the ocean it reacts with CO_3^{2-}, forming HCO_3^-, decreasing the fraction of CO_2 that can be readily absorbed by the oceans. Therefore, because of the buffering capacity of the oceans, a doubling of atmospheric [CO_2] will not correspond to a doubling of [CO_2^*] but instead will result in an increase on the order of 10%. Due to both these chemical and physical changes (e.g., warming and stratification), the oceans may become less efficient in the uptake of

55 anthropogenic CO_2 as the climate continues to change (Sarmiento and Le Quéré, 1996; Matear and
56 Hirst, 1999; Joos et al., 1999; Le Quéré et al., 2010).
57 Numerous experiments and observations indicate that ocean acidification will have significant
58 effects on calcifying marine organisms. For example, the rate of coral reef building may decrease,
59 calcification rates of planktonic cocolithophores and foraminifera may be suppressed, and significant
60 changes in trophic level interactions and ecosystems may occur (Cooley and Doney, 2009; Silverman et
61 al., 2009; Fabry et al., 2008; Riebesell et al., 2000). Some coral reefs are believed to already be eroding
62 for parts of the year due to changes in ocean acidification (Yates and Halley, 2006; Albright et al., 2013).
63 Global surface pH is projected to drop by up to 0.33 units (Gehlen et al., 2014; Orr et al., 2005) and all
64 existing coral reefs will be surrounded by conditions well outside of preindustrial values and even
65 today's saturation levels (Ricke et al., 2013) under the RCP8.5 scenario.
66 These model projections of ocean acidification come primarily from Earth System Models
67 (ESMs) that integrate the interactions of atmosphere, ocean, land, ice and biosphere to estimate the
68 present and future state of the climate. ESMs are computationally expensive and typically run using
69 stylized experiments or a few Representative Concentration Pathways (RCPs), greenhouse gas
70 concentration trajectories used in the Intergovernmental Panel on Climate Change 5th Assessment
71 Report (IPCC, 2013). This generally limits ESM-based analyses to those scenarios. The occurrence of
72 ocean warming and acidification is consistent across the Coupled Model Intercomparison Project
73 (CMIP5) ESMs, but their rates and magnitudes are strongly dependent upon the scenario (Bopp et al.,
74 2013).
75 An alternative to ESMs are reduced-form models, relatively simple and small models that can be
76 powerful tools due to their simple input requirements, computational efficiency, tractability, and thus
77 ability to run multiple simulations under arbitrary future emission pathways. This allows for
78 quantification of arbitrary climate change scenarios, emulation of larger ESMs, as well as in-depth

parameter sensitivity studies and uncertainty analyses (Senior and Mitchell, 2000; Ricciuto et al., 2008; Irvine et al., 2012).

Our goal of this study is to quantify how well Hector, a reduced-form model that explicitly treats surface ocean chemistry, emulates the marine carbonate system of both observations and the CMIP5 archive, and explore the parametric sensitivities to Hector's ocean outputs. The remainder of the paper is organized as follows; section 2, a detailed description of Hector's ocean component, the data sources and simulations run, section 3, results of the model comparison and sensitivity experiments and lastly, section 4, a discussion of the results.

2.0 Model Description – Hector

Hector is open-source and available at https://github.com/JGCRI/hector. The repository includes all model code needed to compile and run the model, as well as all input files and R scripts to process its output. Hector is a reduced form climate carbon-cycle model, which takes in emissions of CO_2, non-CO_2s and aerosols, converts emissions to concentrations where needed, calculates the global radiative forcing and then global mean temperature change. Hector contains a well-mixed global atmosphere, a land component consisting of vegetation, detritus, and soil, and an ocean component. In this study we use Hector v1.1, with an updated ocean temperature algorithm to better match the CMIP5 mean. For a detailed description of the land and atmospheric components of Hector, please refer to Appendix A and Hartin et al., 2015.

2.1 Ocean Component

Hector's ocean component is based on work by Lenton (2000), Knox and McElroy (1984) and Sarmiento and Toggweiler (1984). It consists of four boxes: two surface boxes (high and low latitude), one intermediate, and one deep box. The cold high latitude surface box makes up 15% of the ocean surface area, representing the subpolar gyres (> 55°), while the warm low latitude surface box (<55°)

makes up 85% of the ocean surface area. The temperatures of the surface boxes are linearly related to the global atmospheric temperature change, and are initialized at 2°C and 22°C for the high and low latitude boxes respectively. This temperature gradient sets up a flux of carbon into the cold high latitude box and a flux out of the warm low latitude box. The ocean-atmosphere flux of carbon is the sum of all the surface fluxes (F_i, n=2).

$$F_O\,(t) = \sum_{i=1}^{n} F_i(t) \tag{1}$$

Once carbon enters the high latitude surface box it is circulated between the boxes via advection and water mass exchange, simulating a simple thermohaline circulation. In this version of Hector we do not explicitly model diffusion; simple box-diffusion models and "HILDA" (e.g., Siegenthaler and Joos, 1992) type models are typically in good agreement with observations but are more computationally demanding than a simple box model (Lenton, 2000). The change in carbon of any ocean box *i* is given by the fluxes in and out, with $F_{atm->i}$ as the atmospheric carbon flux of the two surface boxes:

$$\frac{dC_i}{dt} = \sum_{j=1}^{in} F_{j\to i} - \sum_{j=1}^{out} F_{i\to j} + F_{atm\to i} \tag{2}$$

The flux of carbon between the boxes is related to the transport ($T_{i->j}$,$m^3\ s^{-1}$) between *i* and *j,* the volume of *i* (V_i, m^3) *,* and the total carbon in *i* (including any air-sea fluxes) (C_i, Pg C)*;*

$$\frac{dC_i}{dt} = \frac{T_{i\to j} * \ C_i(t)}{V_i} \tag{3}$$

Volume transports are tuned to yield an approximate flow of 100 Pg C from the surface high latitude box to the deep ocean box at steady state, simulating deep water formation.

Hector includes four measurable variables of the carbonate system in seawater: DIC, total alkalinity (TA), pCO_2 and pH, any pair of which can be used to describe the entire carbonate system. DIC and TA are used to solve the surface ocean pH and pCO_2 values. These detailed carbonate chemistry

equations are based on numeric programs from Zeebe and Wolf-Gladrow, 2001 (Appendix B). We simplified the equations by neglecting the effects of pressure, since we are only concerned with the surface ocean. Hector is run to equilibrium in a perturbation-free mode, prior to running the historical period, ensuring that it is in steady state (Hartin et al., 2015; Pietsch and Hasenauer, 2006). DIC (μmol kg^{-1}) in the surface boxes is a function of the total carbon (Pg C) and the volume of the box. All carbon within the ocean component is assumed to be inorganic carbon. Dissolved organic matter is less than 2% of the total inorganic carbon pool, of which a small fraction is dissolved organic carbon (Hansell and Carlson, 2001). Therefore, for simplicity we chose not to include organic carbon within Hector.

TA is calculated at the end of model spinup (running to equilibrium in an a historical, perturbation-free mode) and held constant going forward in time, resulting in 2311.0 μmol kg^{-1} for the high latitude box and 2435.0 μmol kg^{-1} for the low latitude box. These values are within the range of open ocean observations, 2250.0 – 2450.0 μmol kg^{-1} (Key et al., 2004; Fry et al., 2015). We assume negligible carbonate precipitation/dissolution and no alkalinity runoff from the land surface to the open ocean. Alkalinity is typically held constant with time, a reasonable assumption over several thousand years (Lenton, 2000; Zeebe and Wolf-Gladrow, 2001; Glotter et al., 2014; Archer et al., 2009). On glacial-interglacial time scales alkalinity and the dissolution of $CaCO_3$ sediments is an important factor in controlling atmospheric [CO_2] (Sarmiento and Gruber, 2006), and thus on these scales Hector will underestimate the oceanic CO_2 uptake.

Hector solves for pCO_2, pH (total scale), and [HCO_3^-], [CO_3^{2-}], and aragonite (Ω_{Ar}) and calcite saturations (Ω_{Ca}) in both the high and low latitude surface ocean boxes. pCO_2 is calculated from the concentration of [CO_2^*] and the solubility of CO_2 in seawater, based on salinity and temperature. [CO_2^*] is calculated from DIC and the first and second dissociation constants of carbonic acid from Mehrbach et al. (1973), refit by Lueker et al. (2000) (Appendix B).

Carbon fluxes between the atmosphere and ocean are calculated (Takahashi et al., 2009):

$$F = k\,\alpha * \Delta pCO_2 = Tr * \Delta pCO_2 \quad (4)$$

where k is the CO_2 gas-transfer velocity , α is the solubility of CO_2 in seawater (K_0, Appendix B), and the ΔpCO_2 is the difference in pCO_2 between the atmosphere and ocean. The product of k and α results in Tr, the sea-air gas transfer coefficient, where Tr (g C m^{-2} $month^{-1}$ μatm^{-1}) = 0.585 * α * $Sc^{-1/2}$ * U_{10}^2, 0.585 is a unit conversion factor (from mol $liter^{-1}$ atm^{-1} to g-C m^{-3} μatm^{-1} and from cm h^{-1} to m $month^{-1}$) and Sc is the Schmidt number. The Schmidt number (Appendix B) is calculated from Wanninkhof (1992) based on the temperature of each surface box. The average wind speed (U_{10}) of 6.7 m s^{-1} is the same over both surface boxes (Table 1). pH (total scale), [HCO_3^-], and [CO_3^{2-}] are calculated using the [H^+] ion and solved for in a higher order polynomial (Appendix B).

Aragonite and calcite are the two primary carbonate minerals within seawater. The degree of saturation in seawater with respect to aragonite (Ω_{Ar}) and calcite (Ω_{Ca}) is calculated from the product of the concentrations of calcium [Ca^{2+}] and carbonate ions [CO_3^{2-}], divided by the solubility (Ksp). The [Ca^{2+}] is based on equations from Riley and Tongudai (1967) at a constant salinity of 34.5. If Ω = 1, the solution is at equilibrium, and if Ω >1 (Ω <1) the solution is supersaturated (undersaturated) with respect to the mineral.

$$\Omega = \frac{[Ca^{2+}]\,[CO_3^{2-}]}{K_{sp}} \quad (5)$$

2.2. Simulation and experiments

Hector is run under prescribed emissions from 1850-2300 for all four Representative Concentration Pathways (RCP 2.6, RCP 4.5, RCP 6, RCP 8.5) (Moss et al., 2010; van Vuuren et al., 2007). We compare how well Hector can emulate the carbonate system of the CMIP5 median. Our results section will mainly focus on RCP8.5 exploring the response of the carbonate system under a high emissions scenario.

We also ran a series of model sensitivity experiments to quantify how influential some of Hector's parameter inputs are on its outputs (in particular, pH and Ω_{Ar}). Such sensitivity analyses are

important to document model characteristics, explore model weaknesses, and determine to what degree the model behavior conforms to our existing understanding of the ocean system. We do not sample Hector's entire parameter space, a computationally demanding exercise, but instead choose a list of the parameters that we expect, *a priori*, to be important in calculating the marine carbonate system. We selected eight land and ocean parameters, varying each by ±10% relative to the RCP8.5 control, and compare the percentage change from the reference and the perturbation cases in 2005, 2100, and 2300.

2.3 Data Sources

All RCP input emission data are available at http://tntcat.iiasa.ac.at/RcpDb/. Comparison data are obtained from a suite of CMIP5 Earth System Models (Table 2) (Taylor et al., 2012). The CMIP5 output is available from the Program for Climate Model Diagnostics and Intercomparison (http://pcmdi3.llnl.gov/esgcet/home.htm). We took the 0-100m (depth) mean for all available CMIP5 data for six output variables, computing the monthly mean for all years in the historical (1850-2005) and RCP 8.5 (2006-2300) experiments. All outputs were regridded to a standard 1-degree grid using bilinear interpolation in CDO version 1.7.1rc1, and then high latitude (-90 to -55 and 55 to 90 degrees), low latitude (-55 to 55), and global area-weighted means computed using R 3.2.4. All CMIP5 comparisons used in this study are from model runs with prescribed atmospheric CO_2 concentrations. We acknowledge that this is not a perfect comparison, as Hector is emissions-forced being compared to the concentration-forced CMIP5 models, but very few of the latter were run under prescribed emissions. We use a combination of root mean square error (RMSE), rates of change (Δ) and bias (degree of systematic over or underestimation) to characterize Hector's performance relative to the CMIP5 median.

We also compare Hector to a series of observational ocean data. Surface ocean observations of DIC, pCO_2, pH, Ω_{Ar}, and Ω_{Ca} are from time-series stations in both the high and latitude oceans; Hawaii Ocean Time Series (HOT), Bermuda Atlantic Time Series (BATS), the European Station for Time Series in

192 the Ocean at the Canary Islands (ESTOC), the Irminger Sea, and the Iceland Sea (Table 3) . The time-
193 series data are annually averaged over the upper 100m of the water column. The carbonate parameters
194 not found in Table 3 are computed from temperature, salinity, and carbonate parameter pairs using the
195 CO2SYS software (Lewis and Wallace, 1998). Lastly, a longer record (1708 – 1988) of pH and Ω_{Ar} from
196 Flinder's Reef in the western Coral Sea, calculated from boron isotope measurements, is used in the
197 comparison (Pelejero et al., 2005). We use rates of change (Δ) from 1988-2014 similar to BATS and HOT
198 time series, to quantify how well Hector simulates the observed changes in the ocean carbonate
199 parameters (Table 6).
200
201 **3. Results**
202 **3.1 Model and Observation Comparisons**
203 Hartin et al. (2015) conducted a thorough analysis of Hector v1.0 demonstrating that it can
204 reproduce the historical trends and future projections of atmospheric [CO_2], radiative forcing, and global
205 temperature change under the four RCPs. In this study we focus on the upper ocean high and low
206 latitude inorganic carbon chemistry under RCP 8.5.
207 Hector captures the trend in DIC concentrations for both the high and low latitude surface
208 ocean with a global RMSE average of 7.0 μmol kg^{-1} when compared to CMIP5 models over the historical
209 period (Table 4; Figure 2). We note that there is a systematic bias in both the high and low latitude
210 surface boxes when compared to CMIP5. First, he carbon pools of the surface boxes are initialized with
211 carbon values slightly higher than the median CMIP5 values. Second, we note that after 2100 the CMIP5
212 median begins to decline, while Hector rises and stabilizes. Only 3 CMIP5 models ran out to 2300, with
213 one model driving the decline. Regardless, this offset only results in a <3% global difference between
214 CMIP5 and Hector.

Hector accurately tracks the pCO_2 in both the high and low latitude surface ocean with similar rates of change from 1850-2300 (Figure 3). There is a low bias in Hector compared to CMIP5 models after 2100, due to the low bias in projected atmospheric [CO_2] within Hector over the same time period (Hartin et al., 2015). We do find Hector to be in closer agreement with the observation record.

Figure 4 shows the high and low latitude surface pH of Hector compared to CMIP5 and observations from BATS, HOT, ESTOC, Irminger Sea, Iceland Sea, and Flinders Reef. While the high latitude surface pH is slightly higher than the CMIP5 models, Hector is more similar to high latitude observations. Since the preindustrial, observations of surface ocean pH decreased by 0.08 units, corresponding to a 24% increase in [H^+] concentrations and an 8% decrease in [CO_3^{2-}], similar to numerous studies (Feely et al., 2004; Sabine et al., 2004; Caldeira et al., 2003; Orr et al., 2005) that estimate an average global decrease in pH of 0.1 or a 30% increase in [H^+].

The Flinder's Reef pH record provides a natural baseline to compare future trends in ocean acidification. While we did not expect the model to match exactly, as this reef site is heavily influenced by coastal dynamics and internal variability, rates of change from the preindustrial (1750) to 1988 are the same (0.0002 yr^{-1}) for both Hector and Flinder's Reef. Over the limited observational record from both the Pacific and Atlantic Oceans, Hector accurately simulates the decline in pH (-0.0017 yr^{-1}) compared to observations (Table 6). Other observations in the North Pacific show surface changes of pH up to 0.06 units between 1991 and 2006 with an average rate of -0.0017 yr^{-1} (Byrne et al., 2010). Recent work, suggests that the North Atlantic absorbed 50% more anthropogenic CO_2 in the last decade compared to the previous decade, decreasing surface pH by 0.0021 (Woosley et al., 2016). Under RCP 8.5, Hector projects a decrease in low latitude pH of 8.17 in 1850 to 7.77 in 2100 and down to 7.5 by 2300, similar to CMIP5 (Table 5). At approximately 2050, atmospheric [CO_2] is double the preindustrial concentrations, corresponding to a decrease in pH of 7.96. Shortly after this doubling, pH values are well outside the natural variability found in Flinder's Reef.

239 Figure 5, illustrates the high and low latitude surface Ω_{Ar}. We only highlight Ω_{Ar}, as Ω_{Ca} is similar
240 to that of Ω_{Ar}. As with pH, Hector is slightly higher than the CMIP5 Ω_{Ar} median but closer to the
241 observational record. Hector accurately simulates the change in Ω_{Ar} (-0.0090 yr^{-1}) compared to
242 observations (Table 6). Repeated oceanographic surveys in the Pacific Ocean have observed an average
243 0.34% yr^{-1} decrease in the saturation state of surface seawater with respect to aragonite and calcite over
244 a 14-year period (1991-2005) (Feely et al., 2012); the average decrease in Hector is between 0.19% yr^{-1}
245 and 0.25% yr^{-1}. Saturation levels of Ω_{Ar} decrease rapidly over the next 100 years in both the high and
246 low latitude. Hector accurately captures the decline in saturations with low RMSE values for Ω_{Ar}. Under
247 RCP8.5 Hector projects that low latitude Ω_{Ar} will decrease to 2.2 by 2100 and down to 1.4 by 2300. The
248 high latitude oceans will be understaturated with respect to aragonite by 2100 and will drop down to
249 0.7 by 2300.
250 Lastly, Figure 6 highlights pH and Ω_{Ar} projections under all four RCPs from 1850 to 2300. Over
251 the last 20 years, both pH and Ω_{Ar} have declined sharply and will continue to decline under RCP 4.5, 6.0
252 and 8.5, outside of their preindustrial and present day values. These RCPs represent a range of possible
253 future scenarios, with ocean pH varying between 8.15 and 7.46 for the high latitude and Ω_{Ar} varying
254 between 1.94 and 0.60. High latitude Ω_{Ar} saturation levels presently are much lower than the low
255 latitude and reach under saturation before the end of the century. Even under a best-case scenario, RCP
256 2.6, low latitude pH will drop to 7.73 by 2100 and to 7.43 by 2300, with Ω_{Ar} saturations remaining well
257 outside of present day values.
258 **3.2 Model Parameter Sensitivity**
259 Parametric sensitivities are different between pH and Ω_{Ar}, and between the high and low
260 latitude surface ocean boxes. The reference, RCP8.5, refers to the tuned set of parameters found in
261 Hector v1.1, resulting in Figures 2-6. Global pH is fairly insensitive to the values of the input parameters
262 used, while Ω_{Ar} is slightly more sensitive (Table 7). For example, a 10% change in input parameters

results in range from 0.0 - 0.21% in pH and 0.0 - 7.18% in Ω_{Ar}. In comparison a 10% parameter change results in a range from 0.0 - 10.3% in global atmospheric temperature change. In the near term (from 2005-2100) the calculation of pH is sensitive to salinity and beta (terrestrial CO_2 fertilization), while on longer time scales (to 2300), pH is most sensitive to changes in Q_{10} (terrestrial respiration temperature response). Global Ω_{Ar} is most sensitive to changes in salinity in both the near and long term. Similar to pH, Ω_{Ar} becomes more sensitive to changes in Q_{10} in the long term.

Interestingly, the high and low latitude surface boxes respond differently to the same change in input parameters. pH in the high latitude surface ocean is most sensitive to changes in wind stress in the near term. In contrast, in the low latitude surface ocean pH is most sensitive to changes in salinity and beta in the near term. Ω_{Ar} in the both the high and low latitude surface ocean is most sensitive to changes in salinity and temperature in both the near and long term. However, Ω_{Ar} in the low latitude surface ocean becomes more sensitive to Q_{10} after 2100.

4. Discussion

The marine carbonate system is projected to undergo significant changes under the RCPs. pCO_2 and DIC are increasing rapidly as atmospheric [CO_2] continues to rise under RCP 4.5, 6.0 and 8.5. pH, and Ω_{Ar} are decreasing rapidly outside of observations and are projected to continue to decrease under all scenarios (Figure 6). Only under RCP 2.6 do pH and Ω_{Ar} values begin to increase back towards present values. A lowering of Ω_{Ar} from approximately 4.0 to 3.0 is predicted to lead to significant reductions in calcification rates in tropical reefs (Kleypas et al., 1999; Silverman et al., 2009). In agreement with Roy et al., (2015) and Ricke et al., (2013) by the end of the 21st century (2072 under RCP8.5) Hector projects that the low latitude oceans Ω_{Ar} will drop below 3.0, well outside of the preindustrial values of $\Omega_{Ar} > 3.5$. At the end of the 21st Century, the high latitude oceans are close to undersaturation ($\Omega<1$) (Figure 6). However, the threshold for biogenic carbonate precipitation is species dependent and may be

significantly higher than 1.0 when combined with other factors. For example, some coral reef communities need to develop in waters with $\Omega_{Ar} > 3.3$ (Pelejero et al., 2010; Hoegh-Guldberg et al., 2007; Kleypas et al 1999). Accounting for seasonal variations in the Ω_{Ar} saturation levels may move this time of under saturation forward by 17 ± 10 years (Sasse et al., 2015). Due to Hector's time step of 1 year, we may be overestimating the time when ocean acidification reaches a critical threshold. We also note that other factors such as eutrophication, river discharge, and upwelling will likely increase the probability that coastal regions will experience the effects of ocean acidification sooner than the projected open ocean values in Hector (Ekstrom et al., 2015).

In this study we find that pH is fairly insensitive to most parametric changes, but in both the near and long term, pH is sensitive to parameters that indirectly affect atmospheric [CO_2]. Changes in both beta and Q_{10}, (the terrestrial CO_2 fertilization effect and the respiration temperature response, respectively) are responsible for the uptake and release of carbon within the land. Uncertainties in the land carbon cycle have been attributed to uncertainties in future CO_2 projections within the CMIP5 models (Friedlingstein et al., 2014). Therefore, uncertainties in the land carbon cycle will also have implications for the marine carbonate system.

Global Ω_{Ar} saturation levels are most sensitive to changes in salinity. Within Hector, salinity is directly involved in the calculation of [Ca^{2+}]; is used to determine Ω_{Ar}. Typically the carbonate system is normalized to changes in salinity to understand the chemical changes within the system, instead we show that Ω_{Ar} may be sensitive not only to future changes in atmospheric [CO_2] but also sensitive to changes in precipitation and evaporation. This may be important, as studies suggest significant changes in precipitation patterns under a changing climate (Held and Soden, 2006; Liu and Allan, 2013).

The dynamics of ocean uptake of CO_2 are strongly dependent on the rate of downward transport of CO_2 laden waters from the surface ocean to depth. Climate feedbacks on the carbonate system resulting from changes in ocean circulation are neglected in Hector, as the model holds ocean

311 circulation constant in time. CMIP5 models project a weakening in the Atlantic meridional overturning
312 circulation by an average of 36% under RCP8.5 by 2100 (Cheng et al., 2013). We investigate the
313 sensitivity of the carbonate system to a change in ocean circulation by varying the thermohaline
314 circulation parameter (T_t in Figure 1). This parameter represents a portion of the high latitude surface to
315 the deep ocean circulation. A 10% change in ocean circulation (T_t) results in a <4% change in air-sea
316 fluxes and moderate effects on surface pH and Ω_{Ar}. If we scale up from a 10% change in T_t to a 36%
317 change, which is projected from the CMIP5 models, it may result in a roughly 14% change in the air-sea
318 fluxes of carbon to the surface ocean and a 0.3% and 5.0% change in pH and Ω_{Ar}, respectively.
319
320 **6. Conclusions**
321 We developed a simple, open-source, object oriented carbon cycle climate model, Hector, that
322 reliably reproduces the median of the CMIP5 climate variables (Hartin et al., 2015). The ocean
323 component presented in this study, calculates the upper ocean carbonate system (pCO_2, DIC, pH, Ω_{Ar},
324 Ω_{Ca}). Under all four RCPs, pH and Ω_{Ar} decrease significantly outside of their preindustrial values
325 matching both observations and CMIP5. In the near future the open ocean and coral reef communities
326 are likely to experience pH and carbonate saturation levels unprecedented in the last 2 million years
327 (Hönisch et al., 2009).
328 This study is timely because the CMIP5 archive, includes a large suite of ESMs that contained
329 dynamic biogeochemistry, allowing us to study future projections of the marine carbon cycle. Rather
330 than running the ESMs, we can use Hector to quickly emulate the CMIP5 median for projection studies
331 under different emission pathways and sensitivity analyses of the marine carbonate system. Overall, we
332 find that parameters directly involved changes in atmospheric [CO_2] have the most impact on future
333 changes in ocean acidification. Due to Hector's simplistic nature and fast execution times, Hector has

the potential to be a critical tool to the decision-making, scientific, and integrated assessment communities, allowing for further understanding of future changes to the marine carbonate system.

Appendix A: Model Description – carbon cycle

The carbon component in Hector contains three carbon reservoirs: a single well-mixed atmosphere, a land component and an ocean component. The change in atmospheric carbon is a function of the anthropogenic emissions (F_A), land-use change emissions (F_{LC}), and atmosphere-ocean (F_O) and atmosphere-land (F_L) carbon fluxes. The default model time step is 1 year.

$$\frac{dC_{atm}(t)}{dt} = F_A(t) + F_{LC}(t) - F_O(t) - F_L(t) \quad (1)$$

The terrestrial cycle in Hector contains vegetation, detritus, and soil, all linked to each other and the atmosphere by first-order differential equations. Vegetation net primary production is a function of atmospheric CO_2 and temperature. Carbon flows from the vegetation to detritus to soil and loses fractions of carbon to heterotrophic respiration on the way. An 'earth' pool debits carbon emitted as anthropogenic emissions, allowing a continual mass-balance check across the entire carbon cycle. Atmosphere-land fluxes at time t are calculated by:

$$F_L(t) = \sum_{i=1}^{n} NPP_i(t) - RH_i(t) \quad (2)$$

where *NPP* is the net primary production and *RH* is the heterotrophic respiration summed over user-specified n groups (i.e., latitude bands, political units, or biomes) (Hartin et al 2015).

Appendix B: Ocean Carbonate Chemistry

The ocean's inorganic carbon system is solved via a series of equations modified from Zeebe and Wolf-Gladrow (2001). TA and DIC are used to calculate the other variables of the carbonate system:

$$DIC * \left(\frac{K_1}{[H^+]} + 2\frac{K_1K_2}{[H^+]^2}\right) = \left(TA - \frac{K_B B_T}{K_B + [H^+]} - \frac{K_W}{[H^+]} + [H^+]\right) * \left(1 + \frac{K_1}{[H^+]} + \frac{K_1K_2}{[H^+]^2}\right) \quad (1)$$

This equation results in a higher order polynomial equation for H^+, in which the roots (1 positive, 4 negative) are solved for. Once H^+ is solved for, pH, pCO_2, HCO_3^-, and CO_3^{2-} can be determined. We

ignore the nonideality of CO_2 in air and therefore use the partial pressure of CO_2 instead of the fugacity of CO_2. Fugacity is slightly lower by ~0.3% compared to pCO2 (Riebesell et al., 2009; Sarmiento and Gruber, 2006).

$$[CO_2^*] = \frac{DIC}{\left(1 + \frac{K_1}{[H^+]} + \frac{K_1 K_2}{[H^+]^2}\right)} \quad (2)$$

$$pCO_2 = \frac{[CO_2^*]}{K_H} \quad (3)$$

$$[HCO_3^-] = \frac{DIC}{\left(1 + \frac{[H^+]}{K_1} + \frac{K_2}{[H^+]}\right)} \quad (4)$$

$$[CO_3^{2-}] = \frac{DIC}{\left(1 + \frac{[H^+]}{K_2} + \frac{[H^+]^2}{K_1 K_2}\right)} \quad (5)$$

$$K_1 = \frac{[H^+][HCO_3^-]}{[CO_2]} \quad (6)$$

$$K_2 = \frac{[H^+][CO_3^{2-}]}{[HCO_3^-]} \quad (7)$$

K_1 and K_2 are the first and second acidity constants of carbonic acid from Mehrbach et al. (1973) and refit by Lueker et al. (2000).

$$K_B = \frac{[H^+][B(OH)_4^-]}{[B(OH)_3]} \quad (8)$$

K_B is the dissociation constant of boric acid from DOE (1994).

$$K_W = \frac{[H^+]}{[OH^-]} \quad (9)$$

K_W is the dissociation constant of water from Millero (1995).

$$K_{sp} = [Ca^{2+}] * [CO_3^{2-}] \quad (10)$$

Ksp of aragonite and calcite is calculated from Mucci, (1983).

For those equations with multiple coefficients:

1) K_H and K_0 are similar equations calculating Henry's constant or the solubility of CO_2, but they return different units (mol kg^{-1} atm^{-1} and mol L^{-1} atm^{-1}) (see Weiss, 1974 for equations and coefficients). K_H is used to solve pCO_2 while K_0 is used to solve air-sea fluxes of CO_2.
2) The Schmidt number is taken from Wanninkhof (1992) for coefficients of CO_2 in seawater.
3) $[Ca^{2+}]$ (mol kg^{-1}) is calculated from Riley and Rongudai (1967).

Acknowledgements

This research is based on work supported by the US Department of Energy. The Pacific Northwest National Laboratory is operated for DOE by Battelle Memorial Institute under contract DE-AC05-76RL01830.

Author Contributions

C.Hartin designed and carried out the experiments. C. Hartin, B.Bond-Lamberty, and P.Patel developed the model code. A.Mundra process data, design and prepare figures. C.Hartin prepared the manuscript with contributions from all co-authors.

380 **Table 1:** Description and values of ocean parameters in Hector.

Description	Value	Notes
Area of ocean	3.6e14 m^2	Knox and McElroy, 1984
Fractional area of HL	0.15	Sarmiento and Toggweiler, 1984
Fractional area of LL	0.85	Sarmiento and Toggweiler, 1984
Thickness of surface ocean	100 m	Knox and McElroy, 1984
Thickness of intermediate ocean	900 m	
Thickness of deep ocean	2677 m	Total ocean depth 3777m
Volume of HL	5.4e15 m^3	
Volume of LL	3.06e16 m^3	
Volume of IO	3.24e17 m^3	
Volume of DO	9.64e17 m^3	
Surface Area of HL	5.4e13 m^2	
Surface Area of LL	3.06e14 m^2	
Salinity HL and LL	34.5	
Thermohaline circulation (T_T)	7.2e7 m^3s^{-1}	Tuned to give ~100 Pg C flux from surface to deep
High latitude circulation (T_H)	4.9e7 m^3s^{-1}	Tuned to give ~100 Pg C flux from surface to deep
Water mass exchange (intermediate to deep - E_{ID})	1.25e7 m^3s^{-1}	Lenton (2000); Knox and McElroy (1984)
Water mass exchange (low latitude to intermediate - E_{IL})	2.08e7 m^3s^{-1}	Lenton (2000); Knox and McElroy (1984)
Wind speed HL and LL	6.7 m s^{-1}	Takahashi et al., 2009; Liss and Merlivat, 1986

381

Table 2: CMIP5 ESM models used in this study containing ocean carbonate parameters. Ω_{Ar}, Ω_{Ca} were calculated from the model sea surface temperature, sea surface salinity, and CO_3 concentrations.

Model	Model Name	Parameters (RCP 8.5)
BCC-cm1-1	Beijing Climate Center Climate System Model	pCO_2*, temperature
BNU-ESM	Beijing Normal University Earth System Model	pCO_2
CanESM2	Second Generation Canadian Earth System Model	DIC, pH, salinity
CESM1-BGC	Community Earth System Model version 1, Biogeochemistry	CO_3, DIC, pH, salinity
CMCC-CESM	Centro Euro-Mediterraneo sui Cambiamenti Climatici - Carbon Earth System Model	pCO_2, temperature, CO_3, DIC, pH, salinity
CNRM-CM5	National Center for Meteorological Research Climate Model version 5	CO_3, DIC
GFDL-ESM2G	Geophysical Fluid Dynamic Laboratory Earth System Model with GOLD ocean component	pCO_2, temperature, pH, salinity
GFDL-ESM2M	Geophysical Fluid Dynamic Laboratory Earth System Model with MOM ocean component	pCO_2, temperature, CO_3, pH, DIC, salinity
GISS-E2-H-CC	Goddard Institute for Space Studies – HYCOM ocean model with interactive carbon cycle	pCO_2, temperature, DIC, salinity
GISS-E2-R-CC	Goddard Institute for Space Studies – Russell ocean model with interactive carbon cycle	pCO_2, temperature, DIC, salinity
HadGEM2-CC	Hadley Centre Global Environmental Model, version 2 (Carbon Cycle)	pCO_2, temperature, CO_3, DIC, pH, salinity
HadGEM2-ES	Hadley Centre Global Environmental Model, version 2 (Earth System)	pCO_2, temperature, CO_3*, DIC*, pH, salinity
IPSL-CM5A-LR	L'Institut Pierre-Simon Laplace Coupled Model, version 5A, low resolution	Temperature*, CO_3*, DIC*, pH*, salinity*
IPSL-CM5A-MR	L'Institut Pierre-Simon Laplace Coupled Model, version 5A, medium resolution	Temperature, CO_3, DIC, pH, salinity
IPSL-CM5B-LR	L'Institut Pierre-Simon Laplace Coupled Model, version 5A, new atmospherical physic at low resolution	Temperature, CO_3, DIC, pH, salinity
MIROC-ESM	Model for Interdisciplinary Research on Climate, Earth System Model	pCO_2, temperature, salinity
MIROC-ESM-CHEM	Model for Interdisciplinary Research on Climate, Earth System Model, with atmospheric chemistry model	pCO_2, temperature, salinity

MPI-ESM-LR	Max Planck Institute Earth System Model, low resolution	pCO_2*, temperature*, CO_3*, DIC*, pH*, salinity*
MPI-ESM-MR	Max Planck Institute Earth System Model, medium resolution	pCO_2, temperature, CO_3, DIC, pH, salinity
MRI-ESM1	Meteorological Research Institute of Japan – Earth System Model	pCO_2, temperature
NorESM1-ME	Norwegian Earth System Model, version 1, intermediate resolution	pCO_2, temperature, CO_3, DIC, pH, salinity

384 * Variable output to 2300.

385 **Table 3:** Observational time-series information and carbonate parameters from each location.
386

Time-Series Site	Location	Time-Series Length	Reference	Ocean Carbon Parameters	Data Access
BATS	Sargasso Sea	1988-2011	Bates, 2007	TA, DIC	http://www.bios.edu/research/projects/bats
HOT	North Pacific	1988-2011	Dore et al., 2007	TA, DIC, pH, pCO_2, Ω_{Ar}, Ω_{Ca}	http://hahana.soest.hawaii.edu/hot/hot_jgofs.html
ESTOC	Canary Islands	1995-2009	Gonalez-Davila, 2009	TA, pH, pCO_2	http://www.eurosites.info/estoc.php
Iceland Sea	Iceland Sea	1985-2013	Olafsson, 2007a	DIC, pCO_2	http://cdiac.ornl.gov/oceans/Moorings/Iceland_Sea.html
Irminger Sea	Irminger Sea	1983-2013	Olafsson, 2007b	DIC, pCO_2	http://cdiac.ornl.gov/oceans/Moorings/Irminger_Sea.html
Flinders Reef	Coral Sea	1708-1988	Pelejero et al., 2005	pH, Ω_{Ar}	ftp://ftp.ncdc.noaa.gov/pub/data/paleo/coral/west_pacific/great_barrier/flinders2005.txt

387

Table 4: Model validation metrics for the a) high latitude and b) low latitude ocean carbonate variables comparing Hector to CMIP5 from 1850-2004.

a)	**RMSE**	**R2**	**Bias**
DIC	10.00	0.26	47.10
pCO_2	2.65	0.98	-31.78
pH	0.004	0.975	0.061
Ω_{Ar}	0.01	0.98	0.37
Ω_{Ca}	0.02	0.98	0.58

b)	**RMSE**	**R2**	**Bias**
DIC	6.50	0.76	101.28
pCO_2	3.43	0.98	-4.62
pH	0.004	0.966	0.025
Ω_{Ar}	0.02	0.97	0.36
Ω_{Ca}	0.03	0.97	0.53

Table 5: Absolute values and rates of change per year (Δ) for the a) high and b) low latitude surface ocean between 1850, 2100 and 2300 under RCP 8.5 for DIC (μmol kg^{-1}), pCO_2 (μatm), total pH (unitless), Ω_{Ar} (unitless) and Ω_{Ca} (unitless).

	DIC			**pCO2**			**pH**			**Ω_{Ar}**			**Ω_{Ca}**		
a)	**1850**	**2100**	**2300**	**1850**	**2100**	**2300**	**1850**	**2100**	**2300**	**1850**	**2100**	**2300**	**1850**	**2100**	**2300**
Hector	2107.5	2258.1	2335.5	244.7	816.6	1732.1	8.23	7.76	7.46	2.2	1.0	0.6	3.5	1.5	0.9
Δ		0.602	0.387		2.29	4.58		-0.0019	-0.0015		-0.0048	-0.002		-0.008	-0.003
CMIP5	2104.50	2175.79	2243.41	271.62	871.00	1903.82	8.17	7.70	7.38	1.82	0.75	0.44	2.90	1.20	0.70
Δ		0.285	0.34		2.40	5.16		-0.0019	-0.0016		-0.0012	-0.0016		-0.0068	-0.0025

	DIC			**pCO2**			**pH**			**Ω_{Ar}**			**Ω_{Ca}**		
b)	**1850**	**2100**	**2300**	**1850**	**2100**	**2300**	**1850**	**2100**	**2300**	**1850**	**2100**	**2300**	**1850**	**2100**	**2300**
Hector	2073.9	2264.1	2357.6	294.7	879.6	1766.5	8.17	7.77	7.50	4.1	2.2	1.4	6.2	3.3	2.1
Δ		0.76	0.47		2.34	4.43		-0.0016	-0.0014		-0.0076	-0.0040		-0.0116	-0.006
CMIP5	1997.57	2163.16	2298.89	290.47	930.92	1965.23	8.16	7.73	7.45	3.75	2.00	1.36	5.77	3.02	2.04
Δ		0.66	0.68		2.56	5.17		-0.0011	-0.0014		-0.0070	-0.0032		-0.0110	-0.0049

Table 6: Trends and standard error for carbonate system taken from Bates et al., (2014) . Global carbonate system parameters for Hector and CMIP5 from 1988-2014.

	DIC (µmol kg^{-1} yr^{-1})	pCO_2 (µatm yr^{-1})	pH (yr^{-1})	Ω_{Ar} (yr^{-1})
BATS	1.37 ± 0.07	1.69 ± 0.11	–0.0017 ± 0.0001	–0.0095 ± 0.0007
HOT	1.78 ± 0.12	1.72 ± 0.09	–0.0016 ± 0.0001	–0.0084 ± 0.0011
ESTOC	1.09 ± 0.10	1.92 ± 0.24	–0.0018 ± 0.0002	–0.0115 ± 0.0023
Iceland Sea	1.22 ± 0.27	1.29 ± 0.36	–0.0014 ± 0.0005	–0.0018 ± 0.0027
Irminger Sea	1.62 ± 0.35	2.37 ± 0.49	–0.0026 ± 0.0006	–0.0080 ± 0.0040
Hector	0.90	1.82	-0.0017	-0.0089
CMIP5	0.68	1.77	-0.0018	-0.0074

Table 7: Percentage change from reference (RCP8.5) for two Hector outputs a) global pH and b) global Ω_{Ar} for a ±10% change in eight model parameters. Results are shown for three years, 2005, 2100 and 2300.

a) Year	Parameter	+10% change	-10% change
2005	Albedo	0.00	-0.00
2100		0.00	-0.00
2300		0.00	-0.00
2005	Beta	0.03	-0.03
2100		0.10	-0.10
2300		0.10	-0.10
2005	Circulation	0.02	-0.02
2100		0.06	-0.06
2300		0.09	-0.10
2005	Q_{10}	-0.01	0.01
2100		-0.06	0.07
2300		-0.18	0.21
2005	Salinity	-0.05	0.08
2100		0.03	0.01
2300		0.11	-0.07
2005	Climate Sensitivity	-0.01	0.01
2100		-0.05	0.05
2300		-0.14	0.15
2005	Surface ocean	-0.00	0.00
2100	temperature	-0.01	0.01
2300		-0.02	0.03
2005	Wind Stress	-0.02	0.03
2100		-0.05	0.07
2300		-0.09	0.07

b) Year	Parameter	+10% change	-10% change
2005	Albedo	0.01	-0.00
2100		0.01	-0.01
2300		-0.00	0.00
2005	Beta	0.38	-0.40
2100		1.33	-1.34
2300		1.38	-1.35
2005	Circulation	0.41	-0.45
2100		1.01	-1.05
2300		1.48	-1.55
2005	Q_{10}	-0.09	0.10
2100		-0.87	0.95
2300		-2.40	3.00
2005	Salinity	3.80	-4.28
2100		5.60	-5.89
2300		7.17	-7.18
2005	Climate Sensitivity	0.07	-0.07
2100		0.55	-0.56
2300		0.43	-0.27
2005	Surface ocean temperature	2.07	-1.99
2100		2.41	-2.29
2300		2.43	-2.27
2005	Wind Stress	-0.18	0.25
2100		-0.65	0.88
2300		-1.13	0.88

409

Figure 1: Representation of the carbon cycle in Hector. The atmosphere consists of one well-mixed box, connected to the surface ocean via air-sea fluxes of carbon. The terrestrial component consists of user defined biomes or regions for vegetation, detritus, and soil. The earth pool is continually debited to act as a mass balance check on the carbon cycle (Hartin et al., 2015). The ocean consists of four boxes, with advection (represented by solid arrows) and water mass exchange (represented by dashed arrows) simulating thermohaline circulation. The marine carbonate system is solved for in the high and low latitude surface boxes. At steady state, there is a flux of carbon from the atmosphere to the high latitude surface box, while the low-latitude surface ocean releases carbon to the atmosphere.

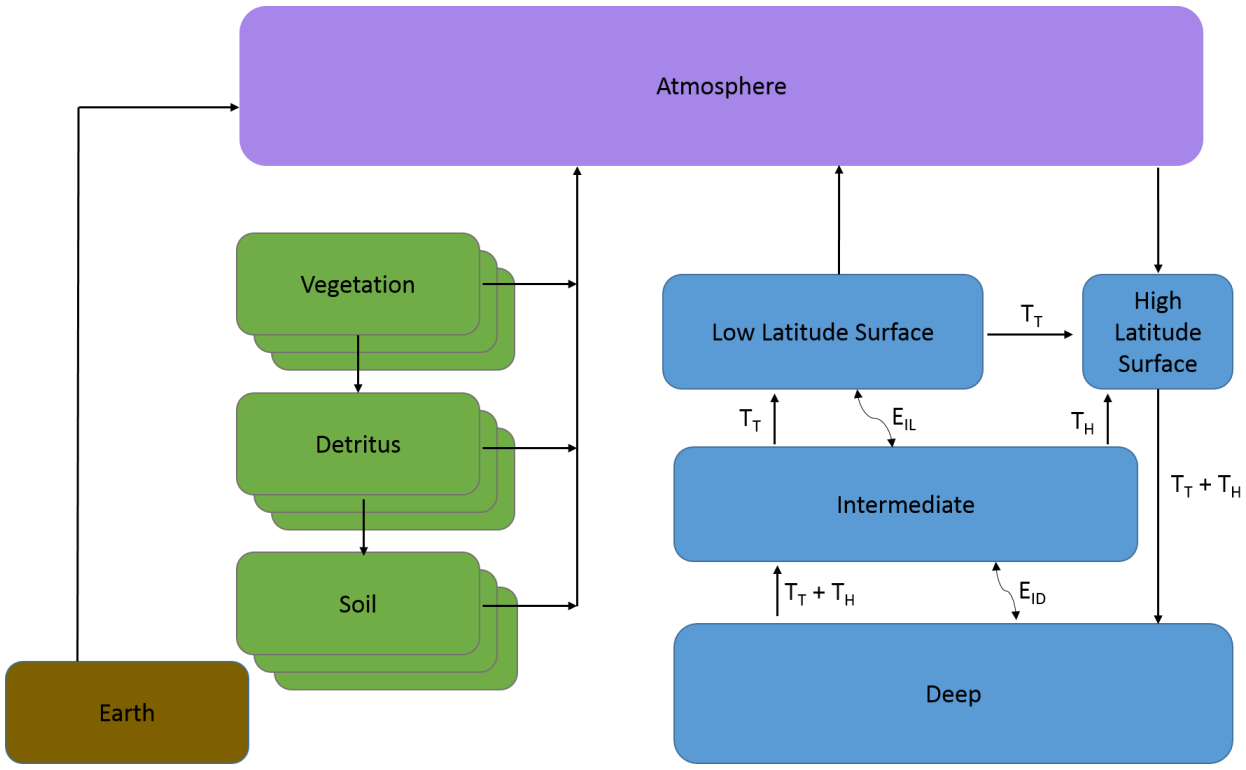

Figure 2: Dissolved inorganic carbon (DIC) for high (top) and low latitude (bottom) surface ocean under RCP 8.5; Hector (blue), CMIP5 median, standard deviation, and model range (red, *n = 15* (1850-2100) and *n= 3* (2101-2300)); and observations from BATS (teal), ESTOC (pink), HOT (purple), Iceland (yellow) and Irminger Sea (navy). Note a doubling of CO_2, from preindustrial values occurs around 2050.

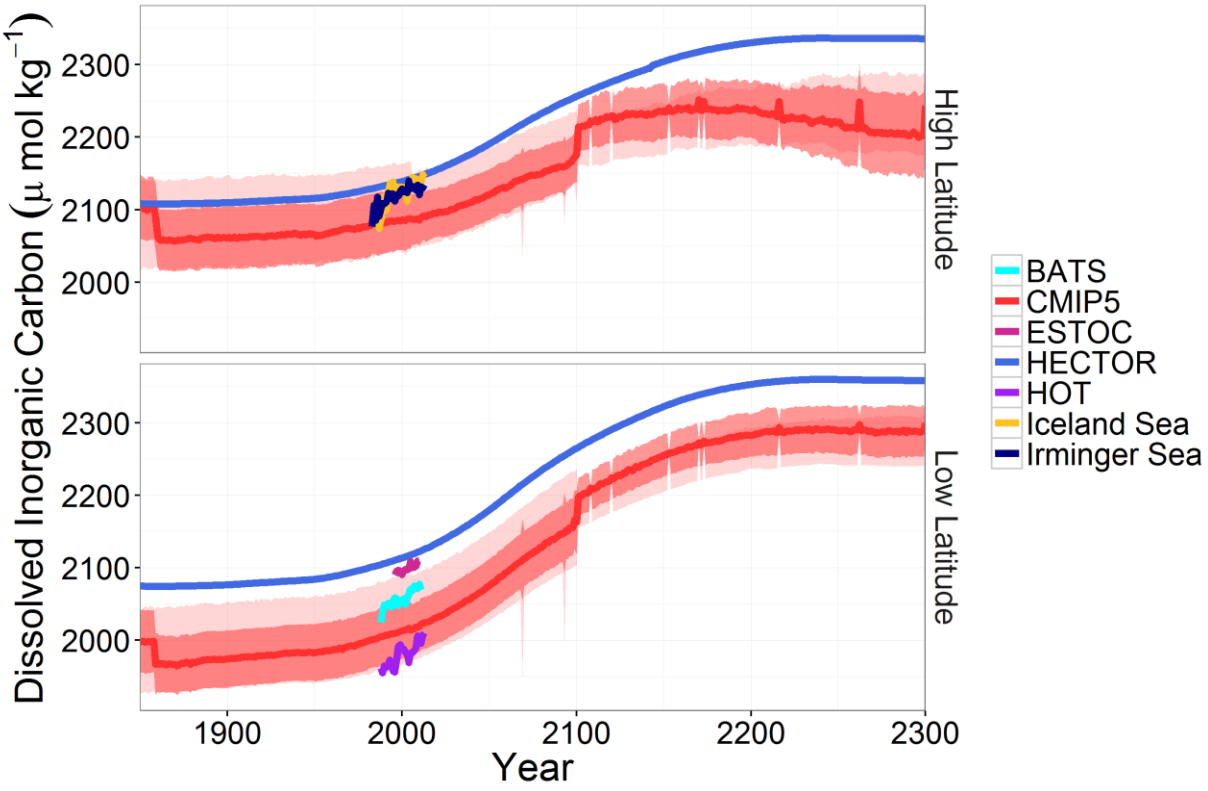

Figure 3: pCO_2 for high (top) and low latitude (bottom) surface ocean under RCP 8.5; Hector (blue), CMIP5 median, standard deviation, and model range (red, *n = 15* (1850-2100) and *n= 2* (2101-2300)); and observations from BATS (teal), HOT (purple), ESTOC (pink), Iceland (yellow) and Irminger Sea (navy).

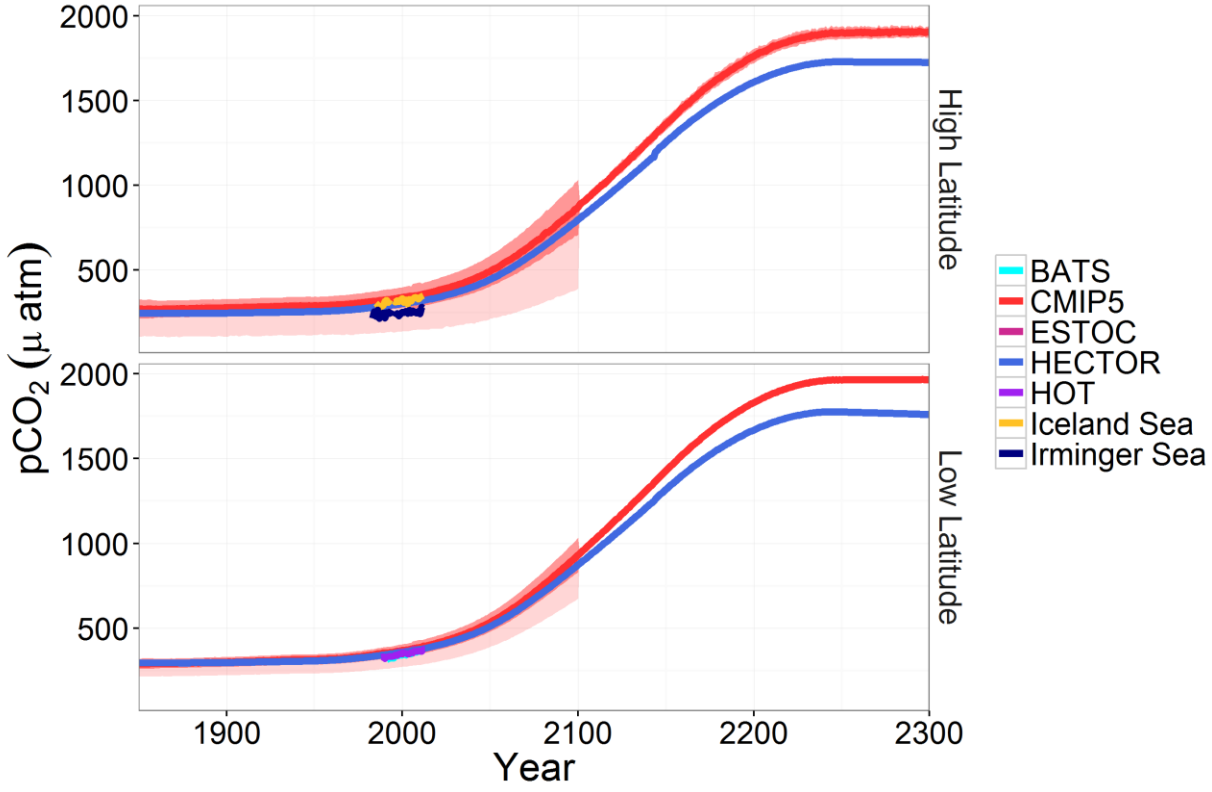

Figure 4: pH for high (top) and low latitude (bottom) surface ocean under RCP 8.5; Hector (blue), CMIP5 median, standard deviation, and model range (red, *n = 13* (1850-2100) and *n= 2* (2101-2300)); and observations from BATS (teal), ESTOC (pink), HOT (purple) Flinder's Reef (green), Iceland (yellow) and Irminger Sea (navy).

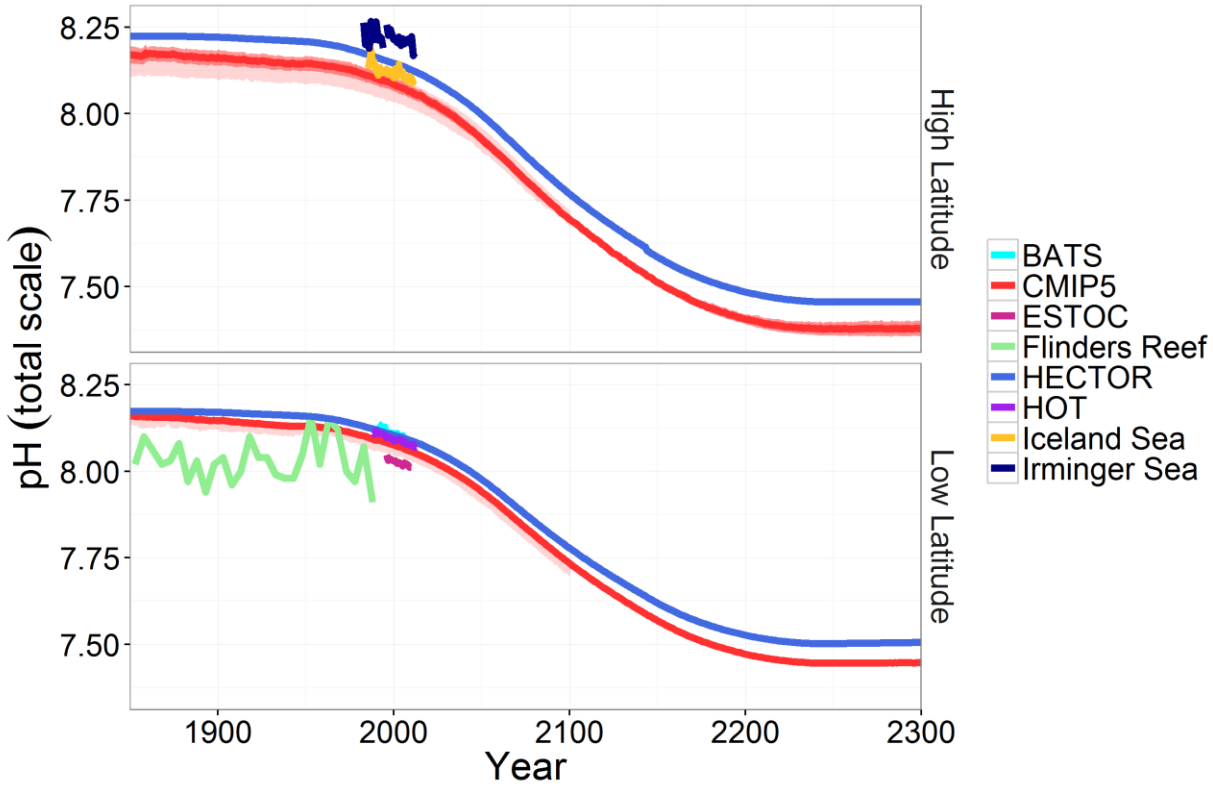

Figure 5: Aragonite saturation (Ω_{Ar}) for high (top) and low latitude (bottom) surface ocean under RCP 8.5; Hector (blue), CMIP5 median, standard deviation, and model range (red, *n = 10* (1850-2100) and *n= 2* (2101-2300)); and observations from BATS (teal), HOT (purple) and Flinder's Reef (green).

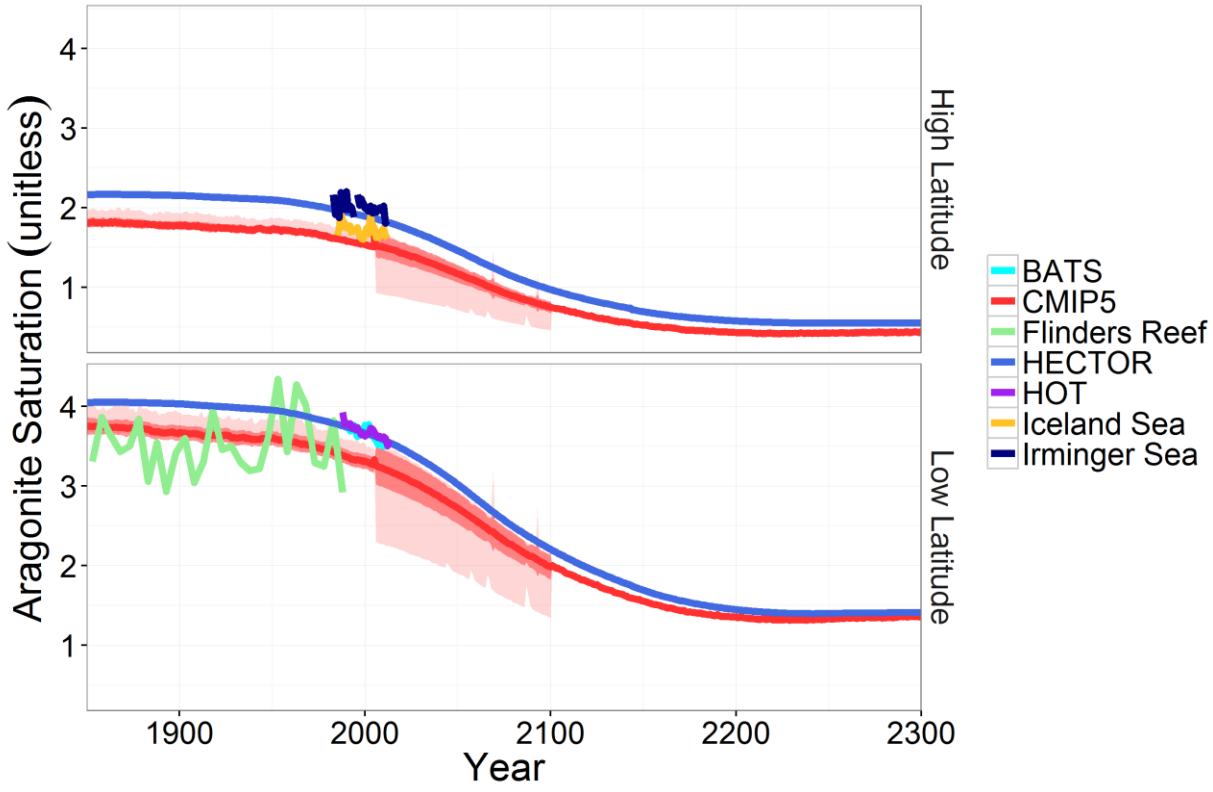

Figure 6: High and low latitude a) pH and b) aragonite saturation (Ω_{Ar}) time series for Hector from 1850-2300 for RCP 2.6 (red), RCP 4.5 (green), RCP 6.0 (teal) and RCP 8.5 (purple). Note that even under a strongly mitigated scenario (RCP 2.6), both Ω_{Ar} and pH at 2300 are still lower than preindustrial values.

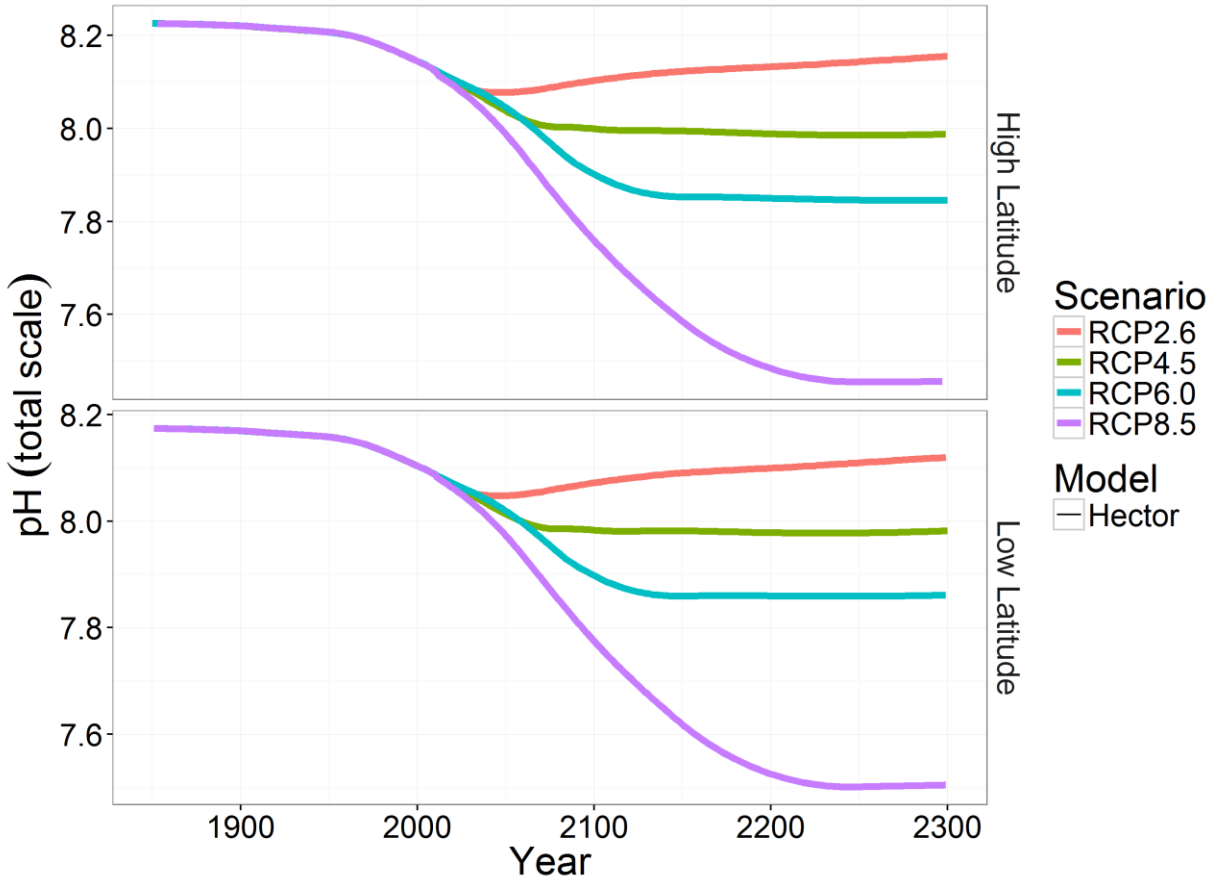

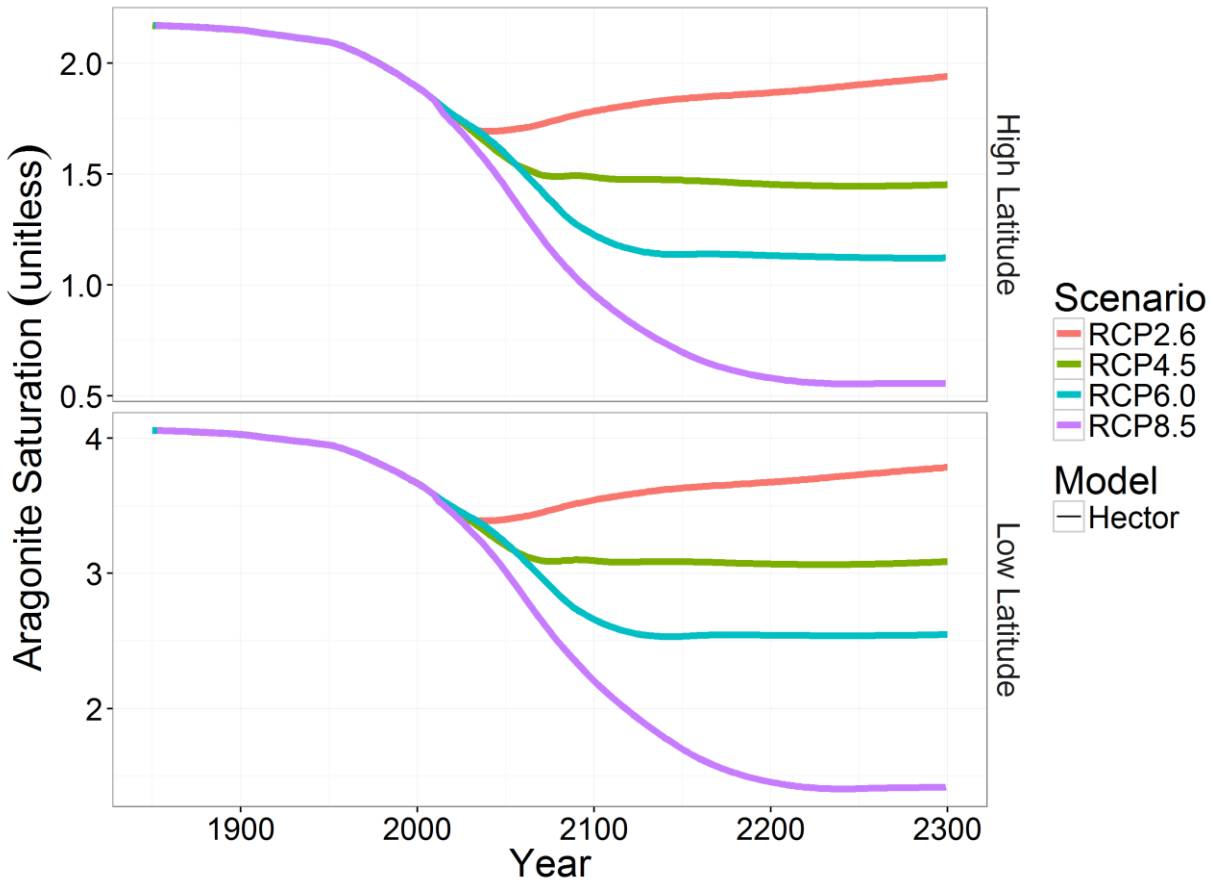
Aragonite Saturation (unitless)
2.0
1.5
1.0
0.5
4
3
2
1900
2000
2100
2200
2300
Year
High Latitude
Low Latitude
Scenario
RCP2.6
RCP4.5
RCP6.0
RCP8.5
Model
Hector

446

447

448 **REFERENCES**

449 Albright, R., Langdon, C., and Anthony, K. R. N.: Dynamics of seawater carbonate chemistry, production,
450 and calcification of a coral reef flat, central Great Barrier Reef, Biogeosciences, 10, 6747-6758,
451 10.5194/bg-10-6747-2013, 2013.
452 Archer, D., Eby, M., Brovkin, V., Ridgwell, A., Cao, L., Mikolajewicz, U., Caldeira, K., Matsumoto, K.,
453 Munhoven, G., Montenegro, A., and Tokos, K.: Atmospheric Lifetime of Fossil Fuel Carbon Dioxide,
454 Annual Review of Earth and Planetary Sciences, 37, 117-134,
455 doi:10.1146/annurev.earth.031208.100206, 2009.
456 Bates, N. R.: Interannual variability of the oceanic CO2 sink in the subtropical gyre of the North Atlantic
457 Ocean over the last 2 decades, Journal of Geophysical Research: Oceans, 112, C09013,
458 10.1029/2006JC003759, 2007.
459 Bates, N. R., Astor, Y. M., Church, M. J., Currie, K., Dore, J. E., Gonzalez-Davila, M., Lorenzoni, L., Muller-
460 Karger, F., Olafsson, J., and Santana-Casiano, J. M.: A time-series view of changing ocean chemistry due
461 to ocean uptake of anthropogenic CO2 and ocean acidification, Oceanography, 27, 126-141,
462 http://dx.doi.org/10.5670/oceanog.2014.16., 2014.
463 Bopp, L., Resplandy, L., Orr, J. C., Doney, S. C., Dunne, J. P., Gehlen, M., Halloran, P., Heinze, C., Ilyina, T.,
464 Séférian, R., Tjiputra, J., and Vichi, M.: Multiple stressors of ocean ecosystems in the 21st century:
465 projections with CMIP5 models, Biogeosciences Discuss., 10, 3627-3676, 10.5194/bgd-10-3627-2013,
466 2013.
467 Byrne, R. H., Mecking, S., Feely, R. A., and Liu, X.: Direct observations of basin-wide acidification of the
468 North Pacific Ocean, Geophysical Research Letters, 37, L02601, 10.1029/2009GL040999, 2010.
469 Caldeira, K., Jain, A. K., and Hoffert, M. I.: Climate Sensitivity Uncertainty and the Need for Energy
470 Without CO2 Emission, Science, 299, 2052-2054, 10.1126/science.1078938, 2003.
471 Cheng, W., Chiang, J. C. H., and Zhang, D.: Atlantic Meridional Overturning Circulation (AMOC) in CMIP5
472 Models: RCP and Historical Simulations, Journal of Climate, 26, 7187-7197, 10.1175/JCLI-D-12-00496.1,
473 2013.
474 Cooley, S. R., and Doney, S. C.: Anticipating ocean acidification's economic consequences for commercial
475 fisheries, Environmental Research Letters, 4, 024007, 2009.
476 DOE: Handbook of methods for the analysis of the various parameters of the carbon dioxide system in
477 sea water, edited by: Dickson, A. G., and Goyet, C., ORNL/CDIAC-74, 1994.
478 Doney, S. C.: The Growing Human Footprint on Coastal and Open-Ocean Biogeochemistry, Science, 328,
479 1512-1516, 10.1126/science.1185198, 2010.
480 Dore, J. E., Lukas, R., Sadler, D. W., Church, M. J., and Karl, D. M.: Physical and biogeochemical
481 modulation of ocean acidification in the central North Pacific, Proceedings of the National Academy of
482 Sciences, 106, 12235-12240, 10.1073/pnas.0906044106, 2009.
483 Ekstrom, J. A., Suatoni, L., Cooley, S. R., Pendleton, L. H., Waldbusser, G. G., Cinner, J. E., Ritter, J.,
484 Langdon, C., van Hooidonk, R., Gledhill, D., Wellman, K., Beck, M. W., Brander, L. M., Rittschof, D.,
485 Doherty, C., Edwards, P. E. T., and Portela, R.: Vulnerability and adaptation of US shellfisheries to ocean
486 acidification, Nature Clim. Change, 5, 207-214, 10.1038/nclimate2508

487 http://www.nature.com/nclimate/journal/v5/n3/abs/nclimate2508.html#supplementary-information,
488 2015.
489 Fabry, V. J., Seibel, B. A., Feely, R. A., and Orr, J. C.: Impacts of ocean acidification on marine fauna and
490 ecosystem processes, ICES Journal of Marine Science: Journal du Conseil, 65, 414-432,
491 10.1093/icesjms/fsn048, 2008.

492 Feely, R. A., Sabine, C. L., Lee, K., Berelson, W., Kleypas, J., Fabry, V. J., and Millero, F. J.: Impact of
493 Anthropogenic CO2 on the CaCO3 System in the Oceans, Science, 305, 362-366,
494 10.1126/science.1097329, 2004.
495 Feely, R. A., Doney, S. C., and Cooley, S. R.: Ocean acidification: present conditions and future changes in
496 a high-CO2 world, Oceanography, 22, 36-47, http://dx.doi.org/10.5670/oceanog.2009.95, 2009.
497 Feely, R. A., Sabine, C. L., Byrne, R. H., Millero, F. J., Dickson, A. G., Wanninkhof, R., Murata, A., Miller, L.
498 A., and Greeley, D.: Decadal changes in the aragonite and calcite saturation state of the Pacific Ocean,
499 Global Biogeochemical Cycles, 26, GB3001, 10.1029/2011GB004157, 2012.
500 Friedlingstein, P., Meinshausen, M., Arora, V. K., Jones, C. D., Anav, A., Liddicoat, S. K., and Knutti, R.:
501 Uncertainties in CMIP5 Climate Projections due to Carbon Cycle Feedbacks, Journal of Climate, 27, 511-
502 526, 10.1175/JCLI-D-12-00579.1, 2014.
503 Fry, C. H., Tyrrell, T., Hain, M. P., Bates, N. R., and Achterberg, E. P.: Analysis of global surface ocean
504 alkalinity to determine controlling processes, Marine Chemistry, 174, 46-57,
505 http://dx.doi.org/10.1016/j.marchem.2015.05.003, 2015.
506 Gehlen, M., Séférian, R., Jones, D. O. B., Roy, T., Roth, R., Barry, J., Bopp, L., Doney, S. C., Dunne, J. P.,
507 Heinze, C., Joos, F., Orr, J. C., Resplandy, L., Segschneider, J., and Tjiputra, J.: Projected pH reductions by
508 2100 might put deep North Atlantic biodiversity at risk, Biogeosciences Discuss., 11, 8607-8634,
509 10.5194/bgd-11-8607-2014, 2014.
510 Glotter, M., Pierrehumbert, R., Elliott, J., Matteson, N., and Moyer, E.: A simple carbon cycle
511 representation for economic and policy analyses, Climatic Change, 126, 319-335, 10.1007/s10584-014-
512 1224-y, 2014.
513 Hansell, D. A., and Carlson, C. A.: Marine dissolved organic matter and the carbon cycle, Oceanography,
514 14, 41-49, 2001.
515 Hartin, C. A., Patel, P., Schwarber, A., Link, R. P., and Bond-Lamberty, B. P.: A simple object-oriented and
516 open-source model for scientific and policy analyses of the global climate system – Hector v1.0, Geosci.
517 Model Dev., 8, 939-955, 10.5194/gmd-8-939-2015, 2015.
518 Held, I. M., and Soden, B. J.: Robust Responses of the Hydrological Cycle to Global Warming, Journal of
519 Climate, 19, 5686-5699, doi:10.1175/JCLI3990.1, 2006.
520 Hönisch, B., Hemming, N. G., Archer, D., Siddall, M., and McManus, J. F.: Atmospheric Carbon Dioxide
521 Concentration Across the Mid-Pleistocene Transition, Science, 324, 1551-1554,
522 10.1126/science.1171477, 2009.
523 IPCC: Climate Change 2013: The Physical Science Basis. Contribution of Working Group I to the Fifth
524 Assessment Report of the Intergovernmental Panel on Climate Change, edited by: Stocker, T. F., D. Qin,
525 G.-K. Plattner, M. Tignor, S.K. Allen, J. Boschung, A. Nauels, Y. Xia, V. Bex and P.M. Midgley Cambridge
526 University Press, Cambridge, United Kindom and New York, NY, USA, 1535 pp., 2013.
527 Irvine, P. J., Sriver, R. L., and Keller, K.: Tension between reducing sea-level rise and global warming
528 through solar-radiation management, Nature Clim. Change, 2, 97-100, doi:10.1038/nclimate1351, 2012.
529 Joos, F., Plattner, G.-K., Stocker, T. F., Marchal, O., and Schmittner, A.: Global Warming and Marine
530 Carbon Cycle Feedbacks on Future Atmospheric CO2, Science, 284, 464-467,
531 10.1126/science.284.5413.464, 1999.
532 Key, R. M., Kozyr, A., Sabine, C. L., Lee, K., Wanninkhof, R., Bullister, J. L., Feely, R. A., Millero, F. J.,
533 Mordy, C., and Peng, T. H.: A global ocean carbon climatology: Results from Global Data Analysis Project
534 (GLODAP), Global Biogeochemical Cycles, 18, GB4031, 10.1029/2004GB002247, 2004.
535 Kleypas, J. A., Buddemeier, R. W., Archer, D., Gattuso, J.-P., Langdon, C., and Opdyke, B. N.: Geochemical
536 Consequences of Increased Atmospheric Carbon Dioxide on Coral Reefs, Science, 284, 118-120,
537 10.1126/science.284.5411.118, 1999.
538 Knox, F., and McElroy, M. B.: Changes in Atmospheric CO2: Influence of the Marine Biota at High
539 Latitude, J. Geophys. Res., 89, 4629-4637, 10.1029/JD089iD03p04629, 1984.

Kump, L. R., Bralower, T. R., and Ridgwell, A. J.: Ocean Acidification in Deep Time, Oceanography, 22, 94-107, 2009.
Le Quéré, C., Takahashi, T., Buitenhuis, E. T., Rödenbeck, C., and Sutherland, S. C.: Impact of climate change and variability on the global oceanic sink of CO2, Global Biogeochemical Cycles, 24, GB4007, 10.1029/2009GB003599, 2010.
Le Quéré, C., Andres, R. J., Boden, T., Conway, T., Houghton, R. A., House, J. I., Marland, G., Peters, G. P., van der Werf, G. R., Ahlström, A., Andrew, R. M., Bopp, L., Canadell, J. G., Ciais, P., Doney, S. C., Enright, C., Friedlingstein, P., Huntingford, C., Jain, A. K., Jourdain, C., Kato, E., Keeling, R. F., Klein Goldewijk, K., Levis, S., Levy, P., Lomas, M., Poulter, B., Raupach, M. R., Schwinger, J., Sitch, S., Stocker, B. D., Viovy, N., Zaehle, S., and Zeng, N.: The global carbon budget 1959–2011, Earth Syst. Sci. Data, 5, 165-185, 10.5194/essd-5-165-2013, 2013.
Lenton, T. M.: Land and ocean carbon cycle feedback effects on global warming in a simple Earth system model, Tellus B, 52, 1159-1188, 10.1034/j.1600-0889.2000.01104.x, 2000.
Liu, C., and Allan, R., P. : Observed and simulated precipitation responses in wet and dry regions 1850–2100, Environmental Research Letters, 8, 034002, 2013.
Lueker, T. J., Dickson, A. G., and Keeling, C. D.: Ocean pCO2 calculated from dissolved inorganic carbon, alkalinity, and equations for K1 and K2; validation based on laboratory measurements of CO2 in gas and seawater at equilibrium, Marine Chemistry, 70, 105-119, 2000.
Matear, R. J., and Hirst, A. C.: Climate change feedback on the future oceanic CO2 uptake, Tellus B, 51, 722-733, 10.1034/j.1600-0889.1999.t01-1-00012.x, 1999.
Mehrbach, C., Culberson, C. H., Hawley, J. E., and Pytkowicz, R. M.: Measurement of the apparent dissociation constants of carbonic acid in seawater at atmospheric perssure, Limnol. Oceanogr., 18, 897-907, 1973.
Millero, F. J.: Thermodynamics of the carbon dioxide system in the oceans, Geochimica et Cosmochimica Acta, 59, 661-677, 10.1016/0016-7037(94)00354-O, 1995.
Moss, R. H., Edmonds, J. A., Hibbard, K. A., Manning, M. R., Rose, S. K., van Vuuren, D. P., Carter, T. R., Emori, S., Kainuma, M., Kram, T., Meehl, G. A., Mitchell, J. F. B., Nakicenovic, N., Riahi, K., Smith, S. J., Stouffer, R. J., Thomson, A. M., Weyant, J. P., and Wilbanks, T. J.: The next generation of scenarios for climate change research and assessment, Nature, 463, 747-756, doi:10.1038/nature08823, 2010.
Mucci, A.: The solubility of calcite and aragonite in seawater at various salinities, temperatures and at one atmopshere pressure, Amer. J. of Science, 283, 781-799, 1983.
Orr, J. C., Fabry, V. J., Aumont, O., Bopp, L., Doney, S. C., Feely, R. A., Gnanadesikan, A., Gruber, N., Ishida, A., Joos, F., Key, R. M., Lindsay, K., Maier-Reimer, E., Matear, R., Monfray, P., Mouchet, A., Najjar, R. G., Plattner, G.-K., Rodgers, K. B., Sabine, C. L., Sarmiento, J. L., Schlitzer, R., Slater, R. D., Totterdell, I. J., Weirig, M.-F., Yamanaka, Y., and Yool, A.: Anthropogenic ocean acidification over the twenty-first century and its impact on calcifying organisms, Nature, 437, 681-686, doi:10.1038/nature04095, 2005.
Pelejero, C., Calvo, E., McCulloch, M. T., Marshall, J. F., Gagan, M. K., Lough, J. M., and Opdyke, B. N.: Preindustrial to Modern Interdecadal Variability in Coral Reef pH, Science, 309, 2204-2207, 10.1126/science.1113692, 2005.
Pietsch, S. A., and Hasenauer, H.: Evaluatin the self-initialization procedure for large-scale ecosystem models., Global Change Biology, 12, 1-12, 2006.
Riahi, K., Rao, S., Krey, V., Cho, C., Chirkov, V., Fischer, G., Kindermann, G., Nakicenovic, N., and Rafaj, P.: RCP 8.5—A scenario of comparatively high greenhouse gas emissions, Climatic Change, 109, 33-57, 10.1007/s10584-011-0149-y, 2011.
Ricciuto, D. M., Davis, K. J., and Keller, K.: A Bayesian calibration of a simple carbon cycle model: The role of observations in estimating and reducing uncertainty, Global Biogeochemical Cycles, 22, GB2030, 10.1029/2006GB002908, 2008.

Ricke, K. L., Orr, J. C., Schneider, K., and Caldeira, K.: Risks to coral reefs from ocean carbonate chemistry changes in recent earth system model projections, Environmental Research Letters, 8, 034003, dio: 10.1088/1748-9326/8/3/034003, 2013.
Riebesell, U., Zondervan, I., Rost, B., Tortell, P. D., Zeebe, R. E., and Morel, F. M. M.: Reduced calcification of marine plankton in response to increased atmospheric CO2, Nature, 407, 364-367, 2000.
Riebesell, U., Körtzinger, A., and Oschlies, A.: Sensitivities of marine carbon fluxes to ocean change, Proceedings of the National Academy of Sciences, 106, 20602-20609, 10.1073/pnas.0813291106, 2009.
Riley, J. P., and Tongudai, M.: The major cation/chlorinity ratios in sea water, Chemical Geology, 2, 263-269, http://dx.doi.org/10.1016/0009-2541(67)90026-5, 1967.
Sabine, C. L., Feely, R. A., Gruber, N., Key, R. M., Lee, K., Bullister, J. L., Wanninkhof, R., Wong, C. S., Wallace, D. W. R., Tilbrook, B., Millero, F. J., Peng, T.-H., Kozyr, A., Ono, T., and Rios, A. F.: The Oceanic Sink for Anthropogenic CO2, Science, 305, 367-371, 10.1126/science.1097403, 2004.
Sabine, C. L., Feely, R., Wanninkhof, R., Takahashi, T., Khatiwala, S., and Park, G.-H.: The global ocean carbon cycle, In State of the Climate in 2010, Global Oceans. Bull. Am. Meteorol. Soc., 92, S100-S108, 10.1175/1520-0477-92.6.S1, 2011.
Sarmiento, J. L., and Toggweiler, J. R.: A new model for the role of the oceans in determining atmospheric PCO2, Nature, 308, 621-624, 1984.
Sarmiento, J. L., and Le Quéré, C.: Oceanic Carbon Dioxide Uptake in a Model of Century-Scale Global Warming, Science, 274, 1346-1350, 10.1126/science.274.5291.1346, 1996.
Sarmiento, J. L., and Gruber, N.: Ocean Biogeochemical Dynamics, edited by: Press, P. U., Princeton NJ, 2006.
Sasse, T. P., McNeil, B. I., Matear, R. J., and Lenton, A.: Quantifying the influence of CO2 seasonality on future aragonite undersaturation onset, Biogeosciences, 12, 6017-6031, 10.5194/bg-12-6017-2015, 2015.
Senior, C. A., and Mitchell, J. F. B.: The time-dependence of climate sensitivity, Geophysical Research Letters, 27, 2685-2688, 10.1029/2000GL011373, 2000.
Siegenthaler, U., and Joos, F.: Use of a simple model for studying oceanic tracer distributions and the global carbon cycle, Tellus B, 44, 186-207, 10.1034/j.1600-0889.1992.t01-2-00003.x, 1992.
Silverman, J., Lazar, B., Cao, L., Caldeira, K., and Erez, J.: Coral reefs may start dissolving when atmospheric CO2 doubles, Geophysical Research Letters, 36, n/a-n/a, 10.1029/2008GL036282, 2009.
Takahashi, T., Sutherland, S. C., Wanninkhof, R., Sweeney, C., Feely, R. A., Chipman, D. W., Hales, B., Friederich, G., Chavez, F., Sabine, C., Watson, A., Bakker, D. C. E., Schuster, U., Metzl, N., Yoshikawa-Inoue, H., Ishii, M., Midorikawa, T., Nojiri, Y., Körtzinger, A., Steinhoff, T., Hoppema, M., Olafsson, J., Arnarson, T. S., Tilbrook, B., Johannessen, T., Olsen, A., Bellerby, R., Wong, C. S., Delille, B., Bates, N. R., and de Baar, H. J. W.: Climatological mean and decadal change in surface ocean pCO2, and net sea–air CO2 flux over the global oceans, Deep Sea Research Part II: Topical Studies in Oceanography, 56, 554-577, http://dx.doi.org/10.1016/j.dsr2.2008.12.009, 2009.
Taylor, K. E., Stouffer, R. J., and Meehl, G. A.: An Overview of CMIP5 and the Experiment Design, Bulletin of the American Meteorological Society, 93, 485-498, 10.1175/BAMS-D-11-00094.1, 2012.
van Vuuren, D., Elzen, M. J., Lucas, P., Eickhout, B., Strengers, B., Ruijven, B., Wonink, S., and Houdt, R.: Stabilizing greenhouse gas concentrations at low levels: an assessment of reduction strategies and costs, Climatic Change, 81, 119-159, 10.1007/s10584-006-9172-9, 2007.
Wanninkhof, R.: Relationship between wind speed and gas exchange over the ocean, Journal of Geophysical Research: Oceans, 97, 7373-7382, 10.1029/92JC00188, 1992.
Weiss, R. F.: Carbon dioxide in water and seawater: the solubility of a non-ideal gas, Marine Chemistry, 2, 203-215, 10.1016/0304-4203(74)90015-2, 1974.
Woosley, R. J., Millero, F. J., and Wanninkhof, R.: Rapid anthropogenic changes in CO2 and pH in the Atlantic Ocean: 2003–2014, Global Biogeochemical Cycles, 30, 70-90, 10.1002/2015GB005248, 2016.

635 Yates, K., and Halley, R.: CO23 concentration and pCO2 thresholds for calcification and dissolution on
636 the Molokai reef flat, Hawaii, Biogeosciences Discussions, 3, 123-154, 2006.
637 Zeebe, R. E., and Wolf-Gladrow, D.: CO2 in Seawater: Equilibrium, Kinetics, Isotopes, Elsevier,
638 Amsterdam, 2001.

639

640